Noname manuscript No.
(will be inserted by the editor)

Large Eddy Simulations of a set of Experiments with Water Spray-Hot Air Jet Plume Interactions

S. Ebrahimzadeh, G. Maragkos, T. Beji · B. Merci

Received: date / Accepted: date

Abstract Large eddy simulations of water spray-hot air jet plume interactions, as obtained with FireFOAM 2.2.x, are presented. Three hot air jet plumes, with thermal powers of 1.6, 2.1 and 2.6 kW, are examined, interacting with a water spray with discharge rate of 0.084 lpm. A systematic comparison between simulations and experiments involving only the hot air jet plumes, the water spray alone and the combination of the two has been performed in order to evaluate the predictive capabilities of FireFOAM. Overall, the code is capable of predicting well the mean values of the hot air jet plumes but deviations are evident for the rms values. Discrepancies in the predictions of the volume fluxes in the near-field for the water spray alone case are observed if the experimentally reported injection angle is used. Improvements are observed if the injection angle is modified based on the experimentally reported data in the near-field. The interactions between the hot air jet plumes and water sprays, are characterized by the location of the interaction region. The interaction boundary moves up from the base of the plume by increasing the convective heat release rates. The simulation results follow the experimental trend but deviate up to 26% due to the differences in the predicted hot air jet plumes and spray characteristics.

Keywords CFD · LES · spray-jet interaction · FireFOAM

S. Ebrahimzadeh
VK Architects & Engineers,
Guldensporenpark 3, 9820 Merelbeke, Belgium
E-mail: setareh.eb@gmail.com

G. Maragkos, T. Beji and B. Merci
Department of Flow, Heat and Combustion Mechanics, Ghent University,
St. Pietersnieuwstraat 41, B-9000 Ghent, Belgium
Tel.: +32 9264 32 90, Fax: +32 9264 35 75
E-mail: Georgios.Maragkos@UGent.be

1 Introduction

Water-based fire suppression systems have been a reliable and effective active fire protection method for industrial, commercial and (increasingly) residential occupancies. Water has a high heat capacity and latent heat of vaporization. In other words, it consumes high amounts of energy to heat up and evaporate. In interaction with fire, this considerable amount of energy is taken from the flame and/or the smoke and as such, water can have a very strong impact on the fire and smoke dynamics [1].

In terms of sprinkler and water mist systems these impacts are different. Sprinklers require the discharge of a large amount of water, predominantly in the form of large droplets while water mist systems require considerably lower amounts of water and contain very fine droplets. Sprinklers fight with fire mainly by wetting the surfaces of the fuel and the surrounding structures. The main suppression mechanisms of water mist systems, on the other hand are removal of the heat from the hot gases, oxygen displacement by water vapor and attenuation of radiation [2]. Among these mechanisms, delivering an adequate amount of water through the fire plume to the burning fuel and surrounding combustibles can be considered as one of the most important key elements. If a sufficient amount of water could be delivered to the burning surfaces, the burning rate is reduced and, by wetting the adjacent combustibles, the flame spread can be stopped or decreased. For water droplets to be able to reach to the surface of a burning fuel, the downward momentum of the spray should be sufficient enough to overcome the upward momentum of the plume. This penetration process of water sprays through a fire plume will determine how fast and how efficient the extinguishment of a fire could be.

Despite the large number of studies on this subject, there are still many uncertainties regarding the effectiveness of water-based fire suppression systems in fire scenarios. The demonstration of such effectiveness requires large-scale experiments which in return require considerable amount of time and money. However, with the continuing advances in computer technology, numerical simulations can be carried out to provide an insight regarding the involved physical phenomena. It is, therefore, essential to have a tool that can effectively simulate the complex dynamics of water sprays. Understanding the characteristics of the water spray-hot air jet plume interaction is important in order to improve fire suppression by water sprays. This understanding involves how the spray momentum, momentum of flame and hot plume, the spray angle, and water flow rate, affect the degree of penetration of water through the fire and consequently the burning of the fuel surface.

A number of studies have employed Computational Fluid Dynamics (CFD) models for water-based fire suppression systems by focusing on, e.g., numerical simulations of water mist systems [3–5], numerical modelling of fire suppression systems [6–8] or spray-plume interaction [9]. Both experimental and numerical studies have been carried out in the past by focusing on sprinkler/water mist systems, buoyant plumes or the interaction between the two. An experimental study was conducted to measure the water spray characteristics near fire sprinklers in [10]. Experimental work and numerical studies have been carried out by focusing on buoyant plumes. Mean and turbulence quantities for a free axi-symmetric hot air turbulent plume were studied experimentally in [11,12]. Both the Reynolds Averaged Navier Stokes(RANS) [13] and the Large Eddy Simulation (LES) ap-

proaches [14–17] and [18,19] have been used in simulations of turbulent buoyant plumes. In [20,21] a reduced-scale experiment of a hot air plume beneath a ceiling with three different convective heat release rates was conducted. Mean and turbulent velocities were measured in the plume and in the ceiling jet. Studies have also been dedicated to the ceiling jet dynamics, discussing the velocities, temperature rises, and thicknesses of steady fire-driven ceiling jet flows in [21–25].

Spray-plume interaction has been studied experimentally in the past in e.g. [20,26–28]. The influence of the fire size and spray strength or the 'convective heat release rate' (HRR) of a turbulent hot air plume on the structure and location of the interaction boundary is investigated in [20,27]. The effects of ceiling clearance, sprinkler type and sprinkler discharge rate on fire protection performance of sprinklers for non-storage occupancies is studied in [28]. Numerical investigations are also carried out regarding the interaction between the water sprays and buoyant gas flows in [9,13,29–32]. The effect of several water spray parameters on fire suppression mechanism and effectiveness is analyzed in [13]. Some studies are also found on the topic of the interaction of water sprays with the hot buoyant smoke/hot air layer [20,26,30,34,45–47]. The effect of various sprays on the ceiling jet temperatures and velocities is studied in [30] where the reduction in plume-induced ceiling jet gas temperatures and velocities was observed. Despite previous efforts, more research is still needed regarding the flow and spray characteristics especially in the context of spray-plume interaction to get better insight in this complex phenomenon. For these studies two approaches can be used: either looking at real fire-driven flows, or relying on non-reactive flows, using for example hot air to simulate the fire source. In the former, the flow is buoyancy-driven, dominated by the buoyant acceleration due to density difference, relatively independent of the initial fuel stream characteristics. In the latter, on the other hand, the apparent convective Heat Release Rate (HRR) is calculated from the mass flow rate and temperature of the hot air stream at the inlet. This is the approach used here. The advantage of this method is that the flows can be studied (and simulated) without the complexities of combustion reactions.

The main goal of this paper is to evaluate the predictive capabilities of the CFD code FireFOAM 2.2.x (https://github.com/fireFoam-dev) when it comes to Large Eddy Simulations (LES) of water spray-hot air jet plume interactions. To avoid the added complexity related to combustion and radiation modelling, the consideration of water spray-hot air jet plume interaction is chosen as a first step of evaluating the code. The application and evaluation of FireFOAM is expected to be useful for fire safety engineers working on real-life applications of fire scenarios involving water spray-hot air jet plume interactions. The study is divided into three parts with assessment of CFD simulations for the three following aspects:

1. thermal plumes in the absence of water,
2. water spray in the absence of thermal plumes, and
3. the interaction between water sprays and thermal plumes.

2 Governing equations

FireFOAM, developed by FM Global, is an object oriented, C++-based, transient solver for fires and turbulent diffusion flames based on the OpenFOAM platform. FireFOAM version 2.2.x, employed in the current study, uses a Favre-filtered fully

compressible flow formulation and solves for the Navier-Stokes equations, along with transport equation for sensible enthalpy [35]:

$$\frac{\partial \overline{\rho}}{\partial t} + \nabla \cdot (\overline{\rho}\widetilde{u}) = \overline{S}_p \tag{1}$$

$$\frac{\partial(\overline{\rho}\widetilde{u})}{\partial t} + \nabla\cdot(\overline{\rho}\widetilde{u}\widetilde{u}) = -\nabla\overline{p} + \nabla\cdot\left[(\mu+\mu_{sgs})\left(\nabla\widetilde{u} + (\nabla\widetilde{u})^T - \frac{2}{3}(\nabla\cdot\widetilde{u})I\right)\right] + \overline{S}_u + \overline{\rho}g \tag{2}$$

$$\frac{\partial(\overline{\rho}\widetilde{h}_s)}{\partial t} + \nabla \cdot (\overline{\rho}\widetilde{u}\widetilde{h}_s) = \frac{\overline{Dp}}{Dt} + \nabla \cdot \left[\overline{\rho}\left(\alpha + \frac{\nu_{sgs}}{Pr_t}\right)\nabla\widetilde{h}_s\right] + \overline{S}_h \tag{3}$$

where ρ is the density, u is the velocity, p is the pressure, μ is the dynamic viscosity, the subscript sgs denotes sub-grid scale quantities, S_u is the rate of momentum gain/loss per unit volume due to the spray, g is the gravitational acceleration, h_s is the sensible enthalpy, α is the thermal diffusivity, Pr_t is the turbulent Prandtl number and S_h is the energy source term due to spray interaction.

The dynamic Smagorinsky model [36] is used to model turbulence, calculating the sub-grid scale viscosity as:

$$\mu_{sgs} = \overline{\rho}(c_s\Delta)^2|\widetilde{S}| \tag{4}$$

where $|\widetilde{S}| = (2\widetilde{S}_{ij}\widetilde{S}_{ij})^{1/2}$, $\widetilde{S}_{ij} = 0.5(\nabla\widetilde{u} + \nabla\widetilde{u}^T)$ and $\Delta = (\Delta x \Delta y \Delta z)^{1/3}$ is the filter size with Δx, Δy and Δz the effective grid mesh spacings. Both the Smagorinsky constant, c_s, and the turbulent Prandtl number, Pr_t, are determined dynamically and vary locally in space and time. The details of the implementation of the models has been previously reported by the authors in [37]. The Smagorinsky constant is not allowed to take negative values, while no upper bound is defined as well. The Pr_t values are clipped between 0.01 and 1 to ensure numerical stability.

The mass source term due to evaporation is calculated as:

$$\overline{S}_p = -\frac{1}{V}\sum \dot{m}_p \tag{5}$$

where V is the cell volume, the summation is over all the particles within the cell and $\dot{m}_p$ is the evaporation rate for a single droplet (see Eq. (12)).

For the water spray modelling, a Eulerian-Lagrangian approach is employed. Considering that the dominant forces on the droplets are the drag force and the gravitational force, the equations describing the particle motion read:

$$\frac{dx_p}{dt} = u_p \tag{6}$$

$$m_p\frac{du_p}{dt} = -\frac{m_p(u_p - \widetilde{u})}{\tau_p} + m_p g\left(\frac{\rho_p - \overline{\rho}}{\rho_p}\right) \tag{7}$$

where m_p and u_p are the particle mass and velocity, respectively, u is the gas phase velocity while ρ_p and ρ are the particle and gas phase densities, respectively.

The source term, $\overline{S}_u$, representing the momentum transferred from the particles to the gas phase, is obtained by summing the forces transferred from each particle in a grid cell and dividing by the cell volume, V as:

$$\overline{S}_u = \frac{1}{V}\sum\left[\frac{m_p(u_p - \widetilde{u})}{\tau_p} - \dot{m}_p(u_p - \widetilde{u})\right] \tag{8}$$

The particle relaxation time, τ_p, is calculated as:

$$\tau_p = \frac{24\rho_p d_p^2}{18\mu C_D Re_p} \tag{9}$$

The drag coefficient, C_D , is calculated as [38]:

$$C_D = \begin{cases} \frac{24}{Re_p}\left(1 + \frac{1}{6}Re_p^{2/3}\right), & Re_p < 1000 \\ 0.424, & Re_p \geq 1000 \end{cases} \tag{10}$$

with the particle Reynolds number, Re_p, defined as:

$$Re_p = \frac{\overline{\rho}|u_p - \widetilde{u}|d_p}{\mu} \tag{11}$$

where μ is the dynamic viscosity of the gas phase.

The mass and energy transfer between the gas and the liquid can be described by the following set of equations [38]:

$$\dot{m}_p = \frac{dm_p}{dt} = -\rho A_p h_m ln(1 + B_M) \tag{12}$$

$$\frac{dT_p}{dt} = \frac{1}{m_p c_{p,liq}}\left[A_p h(\widetilde{T} - T_p)f + \dot{m}_p h_v\right] \tag{13}$$

T_p is the particle temperature, $c_{p,liq}$ is the liquid specific heat, h_v is the enthalpy of vaporization, h is the heat transfer coefficient between the particle and the gas phase and f is a factor which corrects the rate of heat exchange due to the presence of mass transfer calculated as [40]:

$$f = \frac{\beta}{e^{\beta} - 1}, \qquad \beta = -\frac{c_{p,v}\dot{m}_p}{\pi d_p k Nu} \tag{14}$$

The mass transfer coefficient, h_m, is defined as:

$$h_m = \frac{ShD_v}{d_p} \tag{15}$$

where D_v is the vapor diffusivity.

The Sherwood number is calculated as:

$$Sh = 2 + 0.6Re_p^{1/2}Sc^{1/3} \tag{16}$$

where $Sc = \mu/(\rho D)$ is the Schmidt number while B_M is the Spalding mass transfer number:

$$B_M = \frac{X_{v,s} - X_v}{1 - X_{v,s}} \tag{17}$$

where X_v is the vapor mole fraction in the gas phase and $X_{v,s}$ is the vapor mole fraction at the particle surface obtained from Raoult's law as:

$$X_{v,s} = X_{liq}\frac{p_{sat}}{p} \tag{18}$$

with X_{liq} the liquid volume fraction, p_{sat} the saturation vapor pressure and p the gas phase pressure.

The Nusselt number is obtained from the Ranz-Marshall correlation as [39]:

$$Nu = \frac{hd_p}{k} = 2 + 0.6Re_p^{1/2}Pr^{1/3} \tag{19}$$

with the Prandtl number calculated as $Pr = \mu c_p/k$ and all properties evaluated at the film temperature using the 1/3 rule (i.e. $T_f = (2T_p + T)/3$).

Finally, the source term in the energy equation is calculated as:

$$\overline{S}_h = -\frac{1}{V}\sum\left[\dot{m}_p h_v(T_p) + hA_p(\widetilde{T} - T_p)f\right] \tag{20}$$

with the summation performed over all the particles within the cell.

An explicit solution method is used for the particle mass equation, ensuring that the time step is not larger than an equivalent relaxation time, so that the mass will not become negative. A similar procedure is also applied for the solution of the momentum and energy equations for the particles. Particle tracking is done through the Face-to-Face algorithm [41]. The interpolation of the filtered quantities at the particle position is done through a first-order linear interpolation scheme. More details regarding the solution procedure in terms of spray modelling within the OpenFOAM framework can be found in [42,43].

3 Experimental setup

The case considered is the experiments carried out by Zhou [20,21]. In this small-scale experiment a finely atomized solid cone spray pattern is produced. Although the nozzle is different from a sprinkler, it satisfied the purpose of the small-scale test, namely to extend the existing studies of the interaction between hot air jet plumes and water sprays, specially regarding the influence of the water sprays on the induced ceiling flows driven by strong plumes (from, e.g., rack storage fires). The reason that the experiment is used for this study, is that it provided data for the flow-field for a range of conditions, the water sprays and the interaction between the two. The experimental setup, shown in Figure 1, consisted of a 72 mm diameter nozzle, providing a hot air source, with an aluminum ceiling plate with dimensions of 1.22 m x 1.22 m placed at height 590 mm above the nozzle. Hot air with a temperature of 205 ^{o}C was issued through the nozzle. The ambient temperature was 20 ^{o}C. A range of hot air flows were generated by changing the exit velocity and maintaining a constant exit air temperature. The measured thermal powers of the jet plumes, named here as convective heat release rates, were 1.6 kW, 2.1 kW and 2.6 kW, corresponding to the maximum exit velocities of 3.3 m/s (Re=6800), 4.2 m/s (Re=8700) and 5.3 m/s (Re=11000), respectively. Seeding oil droplets, along with particle image velocimetry (PIV), were employed for measuring the gas phase velocities. No experimental uncertainties were reported by Zhou [14-15]. Nevertheless, errors in the order of 5% for the mean and 20% for the rms values are used here for comparison purposes only. The second part of the experiment included a nozzle below the ceiling with focus on the water spray only, excluding the hot air source. The nozzle used was full cone with 30^o initial spray cone angle. It was installed at y = 560 mm above the hot air nozzle and 30 mm below the center of the aluminum ceiling plate. The water spray nozzle was operated at a pressure of 750 kPa and the measured water flow rate was 0.084

lpm. Shadowgraph imaging was used to measure the spray droplet velocities and diameters. The last part of the experiment consisted of combining both the hot air jet plumes with the water spray. A more detailed description of the experimental set-up can be found in [20, 21].

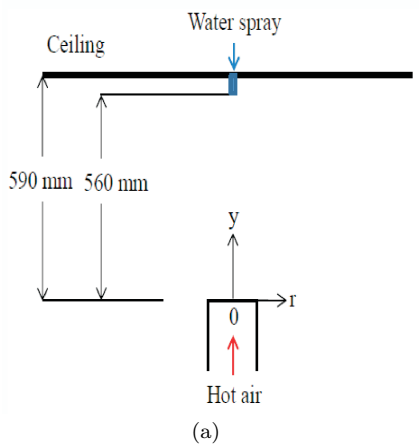

Fig. 1 Schematic of the experimental setup.

4 Numerical setup

A cylindrical computational domain of dimensions (diameter x height) 1 m x 0.662 m is used to simulate the case (Figure 2). The fuel inlet (D=0.072 m) is raised one inlet diameter to reduce the influence from the bottom boundary of the computational domain. The ceiling, placed 0.59 m away from the fuel inlet, is maintained at a constant temperature of 54 ^{o}C for the hot air jet plume cases, based on what was reported experimentally, while an adiabatic boundary condition is assigned for the remaining cases. Nevertheless, the use of either a constant value or an adiabatic boundary condition at the ceiling did not have any substantial influence on the simulation results [44]. The mesh is refined on the centerline and below the ceiling, i.e., in the regions where accurate prediction of the hot air jet plumes is needed. The mesh size in the refined regions is 3 mm, while approximately 6 mm in the rest of the domain. Additional refinement has been performed 1 cm below the ceiling, with the cell sizes decreasing from 3 mm to 1 mm normal to the wall in order to achieve good resolution near the wall based on [44]. The resulting number of cells across the fuel inlet is 24 while the total number of cells used in the simulations is 665000.

For the cases involving the hot air jet plumes, a uniform fixed value of 3.3 m/s (1.6 kW), 4.2 m/s (2.1 kW) and 5.3 m/s (2.6 kW) is applied for velocity at the inlet. To excite turbulence in the flow, 2% [44] random velocity fluctuations are added at the inlet. The present method is currently the only available option in the official OpenFOAM platform. A variable time step is used in the simulations, setting

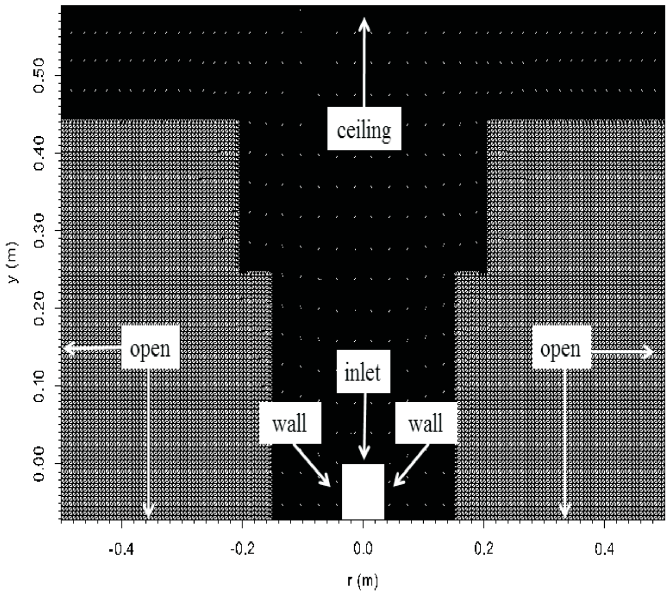

Fig. 2 Computational mesh used in the numerical simulations.

the maximum Courant number to 0.9. The governing equations are advanced in time using a first order implicit Euler scheme. The convective terms are second order centrally differenced. For scalar transport, a second order TVD scheme with a Sweby limiter is used, while the diffusive terms are centrally differenced and corrected for the non-orthogonality of the mesh.

For the cases involving the water sprays, each individual particle is tracked in space and time. Tracing every single droplet is an extremely time consuming task. Therefore, the concept of 'parcel' is introduced, representing several real droplets with identical properties, such as position, velocity and diameter. Based on [44], injecting 100000 parcels per second is sufficient to accurately represent the water spray. In the present study, all parcels contain the same amount of liquid mass. Therefore, parcels with smaller diameter contain more droplets compared to the ones with larger diameter. The spray is assumed to be dilute. Two-way coupling of the gas phase and the dispersed phase is therefore assumed: the influence of the particle phase on the fluid flow is accounted for, but there is no inter-particle interaction and thus collisions, atomization and breakup are not considered. The droplets were distributed within the specified spray angle with a pattern resembling a uniform distribution. The use of a dispersion model, i.e., the effect of continuous phase turbulence fluctuations on the transport of discrete phase particles was originally tested but did not have any significant influence on the predictions, hence, was not taken into account here. Droplets are assumed to be spheres. As part of a sensitivity study, the influence of the specified injection angle (i.e. 30^o and 60^o full cone) and spray pattern (i.e., uniform-like versus Gaussian-like), which determines how the droplets are distributed within the specified spray angle, is investigated. Details regarding the two different spray patterns used in the present study can be found in [44].

The particle injection velocity is calculated as:

$$u_p = \frac{\dot{V}_w}{A_o c_d} \tag{21}$$

where $\dot{V}_w$ is the volumetric flow rate of water, A_o is the orifice area and c_d is the discharge coefficient. With an orifice diameter of 0.33 mm (according to the nozzle manufacturer) and an assumed discharge coefficient of 0.62 [33] the resulting injection velocity is 26.2 m/s.

A Rosin-Rammler distribution is used for the particle initial size distribution:

$$d_p = d_{p,min} + d_{p,m}[-log(1 - yK)]^{1/n} \tag{22}$$

with

$$K = 1 - e^{-\left(\frac{d_{p,max} - d_{p,min}}{d_{p,m}}\right)^n} \tag{23}$$

where $d_{p,min} = 12\ \mu m$, $d_{p,max} = 176\ \mu m$ and $d_{p,m} = 56\ \mu m$ are the minimum, maximum and volume mean median diameter, respectively, and $n = 2$ is the spreading factor [33]. These values have been obtained from the experimental data at 30 mm below the nozzle.

5 Hot air jet plumes

Results for the mean and rms axial velocities at heights y/D=1 and y/D=6 are presented in Figures 3-4. Overall, the magnitude of the mean axial velocities close to the inlet, at height y/D=1, is well predicted. The radial profiles obtained from the simulations are in reasonable agreement with the experiments, however, they are slightly wider than in the experiments. A possible reason could be the fact that no velocity profile was assigned at the inlet (i.e., use of a uniform profile). The rms velocities are slightly under-predicted, failing to capture the peaks observed in the shear layer between the hot air jet plume and the surrounding air. Further downstream, at height y/D=6, both the magnitude of the mean axial velocities and their corresponding radial profiles are quite well predicted (although the profiles are still slightly wide). The velocity fluctuations are now slightly over-predicted for all three cases, with increasing discrepancies from the 1.6 kW to the 2.6 kW case.

The method for generating inlet velocity fluctuations will have an influence on the numerical predictions to some extent since it will determine how turbulent the jet plumes will be and at what axial location they will break. To examine whether the positions where the jet plumes break are correctly captured in the simulations, the predicted mean and rms axial velocities on the centerline are presented in Figure 5. It is clearly observed that the predicted axial velocities are well predicted by the simulations and remain within reasonable uncertainty from the experimental data. The rms values are systematically under-predicted close to the inlet while slightly over-predicted higher in the domain (i.e., at heights y>300 mm). This implies that the jet plumes at these heights in the simulations are more turbulent than the experiments. The ratio of sub-grid scale to molecular viscosity (not shown here) was relatively low at heights y<300 mm and remained less than 0.2 increasing up to about 1.6 just below the ceiling. To some extent, this indicates

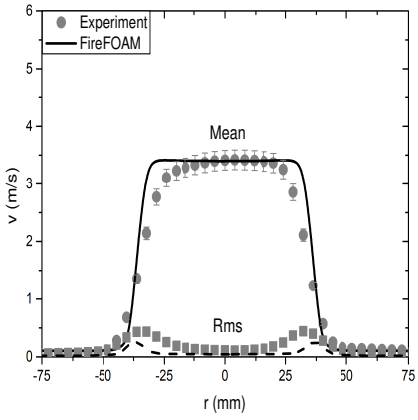

(a)

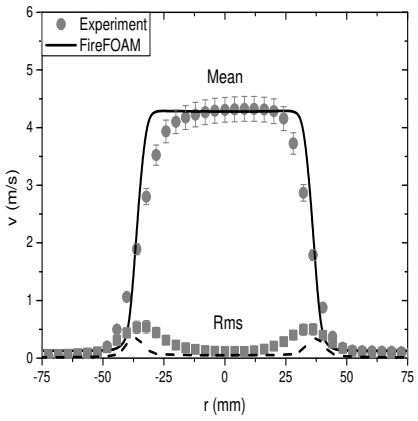

(b)

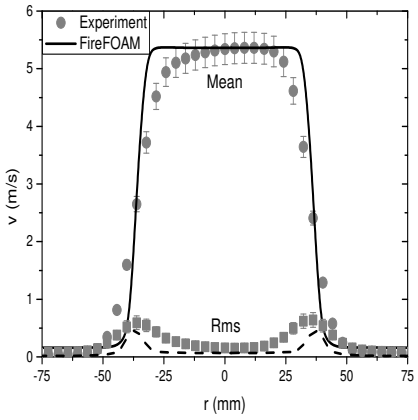

(c)

Fig. 3 Mean and rms axial velocities at y/D=1 for (a) 1.6, (b) 2.1 and (c) 2.6 kW.

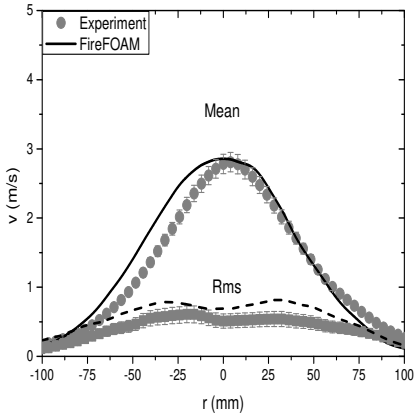

(a)

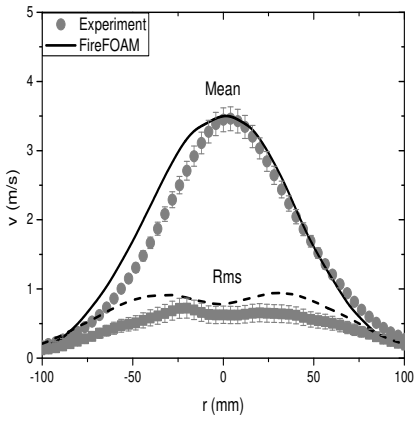

(b)

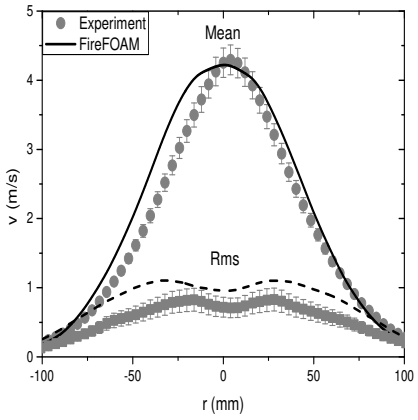

(c)

Fig. 4 Mean and rms axial velocities at y/D=6 for (a) 1.6, (b) 2.1 and (c) 2.6 kW.

that the turbulence resolution is at acceptable levels and even though turbulence modelling is still important in this case, the added sub-grid scale viscosity remained in the same order of magnitude as the molecular one. It is believed that a more sophisticated method for generating inlet velocity fluctuations could possibly improve the predictions in the rms velocities in the numerical simulations. This is considered as future work. For completeness, the centerline evolution of the turbulent Prandtl number (not shown here) varied with axial location, having values of approximately 0.4 close to the inlet and increased to about 0.6 just below the ceiling.

Results from the predicted ceiling jet velocities in the numerical simulations are presented in Figure 6 at locations r=100-300 mm. Overall, there is good agreement between the simulations and the experimental data indicating that the CFD code with the chosen models and given numerical set-up is able to accurately simulate the ceiling jet flow in this case. Nevertheless, the focus of the present study is mainly the interaction of water spray-hot air jet plume interactions. Hence, a detailed analysis for the ceiling jet flow is not presented here.

6 Water spray

Figures 7-8 present results for the volume fluxes, axial velocities and volume mean diameters for water spray simulations at two different locations (i.e., near field (y=530 mm) and far field (y=260 mm)). The injection angle in the experiments was reported to be 30^o (full cone) [20, 21]. Nevertheless, transforming the radial distances in the near field region of the experimental measurements for the volume fluxes (chosen as a parameter since the presence of volume fluxes at a location indicate the presence of water spray as well) into injection degrees, an angle of approximately 60^o is obtained. To examine the influence of the injection angle in the numerical simulations, an additional simulation with an injection angle of 60^o was performed for comparative purposes. It is evident that the simulation results with an injection angle of 30^o deviate significantly from the experimental data in the near field (Figure 8). Narrower profiles for both the volume fluxes and the axial velocities are predicted in the near field and even though the magnitude of the axial velocity is well-predicted, the magnitude of the volume fluxes is strongly over-predicted by approximately 250%. The volume mean diameters around the centerline are well predicted. Nevertheless, the profiles are again narrower when compared to the experiments. The use of a larger injection angle (60^o) not only improves the predicted volume fluxes in the near field, which now compare very favorably with the experiments, but also results in wider profiles for the axial velocities and the volume mean diameters. Nevertheless, discrepancies in the dv50 profiles are evident with the simulations predicting larger droplets with increasing radial distance in contrast to the experiments. The influence of the injection angle in the results for the far field, presented in Figure 9, is less substantial when compared to the near field. Nevertheless, as expected, the higher injection angle (60^o) results in lower volume fluxes and lower axial velocities on the centerline when compared to an injection angle of 30^o. This is not surprising since changing the injection angle results in a change in the momentum of the injected water spray. In general, there is a clear trend of under-predicting the experimental measurements when an injection angle of 60^o is used, while over-predicting them when 30^o is used.

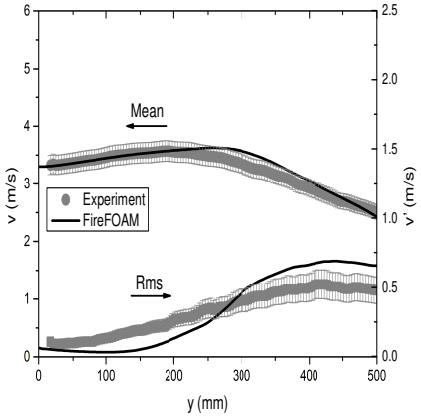

(a)

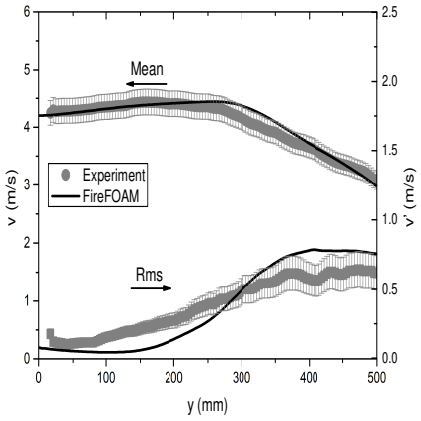

(b)

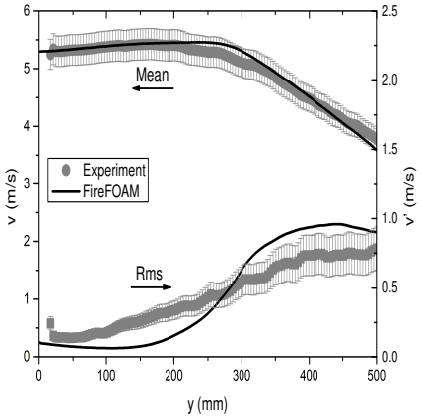

(c)

Fig. 5 Mean and rms axial velocities on the centerline for (a) 1.6, (b) 2.1 and (c) 2.6 kW.

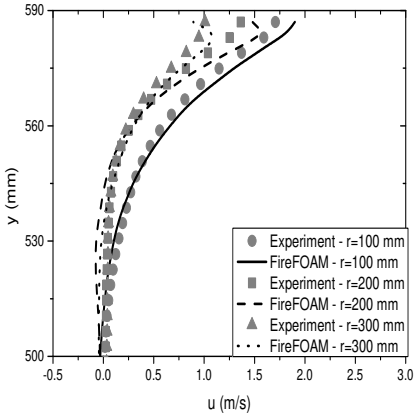

(a)

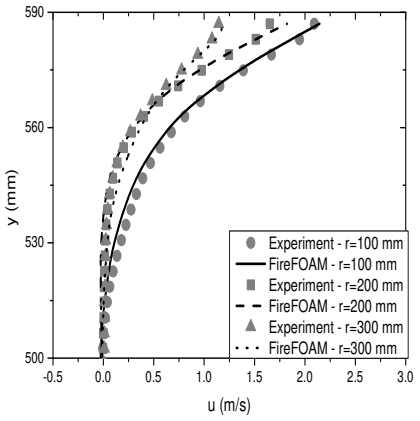

(b)

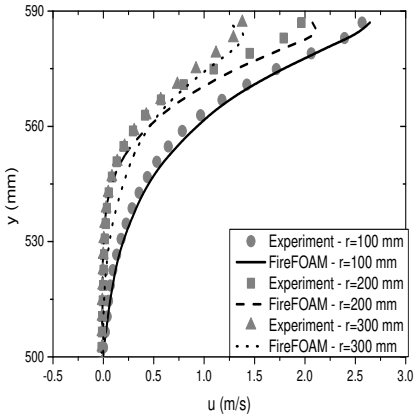

(c)

Fig. 6 Horizontal velocities below the ceiling at various radial locations for (a) 1.6, (b) 2.1 and (c) 2.6 kW.

The overall trends for the dv50 results are qualitatively captured. However, the predictions with the 30^o injection angle, particularly on the centerline, are closer to the experiments when compared to the higher injection angle. Further research related to the injection method of droplets and the droplet distribution within the spray angle would be needed in order to understand the discrepancies observed between the numerical simulations and the experiments. Finally, the spray pattern also has a substantial influence on the spray predictions, particularly for the volume fluxes and the axial velocities. The use of a Gaussian-like spray distribution, concentrating the droplets more on the centerline, results in over-estimations of the volume fluxes and the axial velocities in both the near and far field, regardless of the injection angle used in the numerical simulations. The influence of the spray pattern on the predicted volume mean diameters, even though noticeable, remains smaller. Similar conclusions on the same test case have been previously reported with the use of another CFD software (i.e., the Fire Dynamics Simulator (FDS)) by Beji et al. [5].

7 Spray - plume interactions

A qualitative comparison for the spray-plume interaction between the simulations is given in Figures 9-10. The concept of the 'interaction boundary' is used, which represents a boundary between the downward spray momentum and the upward jet plume momentum. The position of the interaction boundary is determined as the location where the downward flow of air entrained with the spray and the upward buoyant jet plume form a stagnation plane where the two flows meet [32] (i.e., zero vertical velocity on the centerline). Based on the results for the water spray alone, presented in the previous section, a'Uniform' spray pattern was used in the numerical simulations. The results for both injection angles of 30^o and 60^o are presented here.

The interaction boundary planes in the experiments are located at approximately y=60 mm, y=320 mm and y=440 mm for the 1.6, 2.1 and 2.6 kW test cases, respectively. The resulting interaction boundaries in the simulations with the 60^o injection angle are located at approximately y=57 mm (-5%), y=240 mm (-25%) and y=325 mm (-26%), respectively. The resulting interaction boundaries in the simulations with the 30^o injection angle are located at approximately y=47 mm (-21.6%), y=84 mm (-73.7%) and y=137 mm (-68.8%), respectively. It is clear that the predictions with the higher injection angle agree better with the experimental data. Any discrepancies are attributed to possible deficiencies in the gas (i.e., method of turbulent fluctuations at the inlet) and liquid (i.e., dispersion and evaporation modelling) phase modelling, which should be considered in future simulations. Overall, the trend observed in the experiments, i.e., the interaction boundary moving further downstream with increasing convective heat release rate of the plume, is reproduced by the simulations. However, the location of the interaction boundaries is consistently under-predicted in the simulations. Based on the inputs used in the numerical simulations, the initial momentum of the hot air plumes and of the water sprays can be estimated.

The initial momentum of the hot air plume, M_a, without spray is estimated as:

$$M_a = \rho_a A_{nozzle} v_a^2 \tag{24}$$

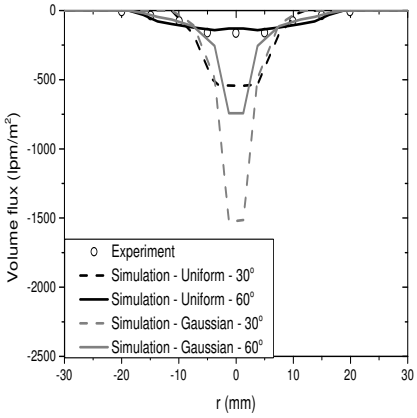

(a)

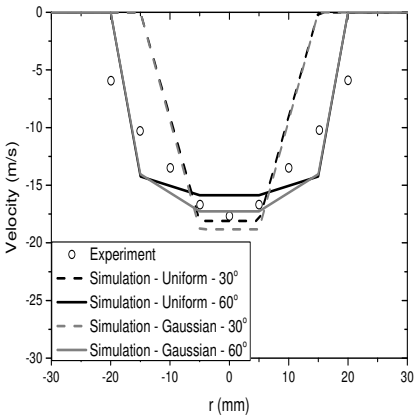

(b)

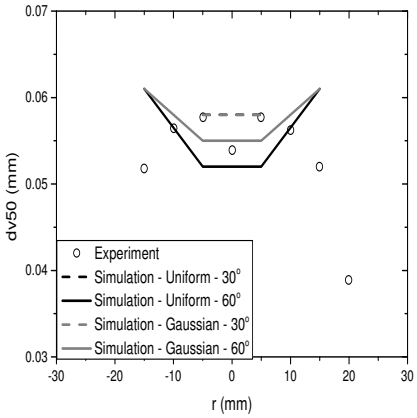

(c)

Fig. 7 Radial profiles of (a) volume flux, (b) axial velocity and (c) volume mean diameter of water droplets in the near field (y=530 mm)

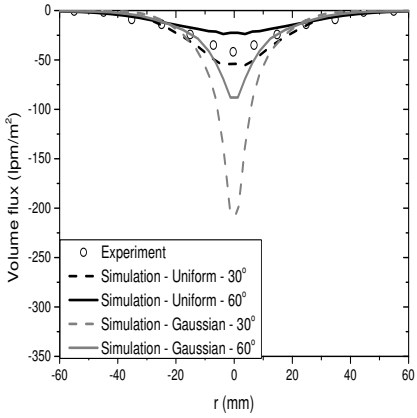

(a)

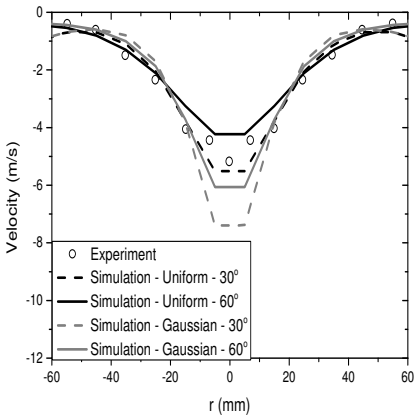

(b)

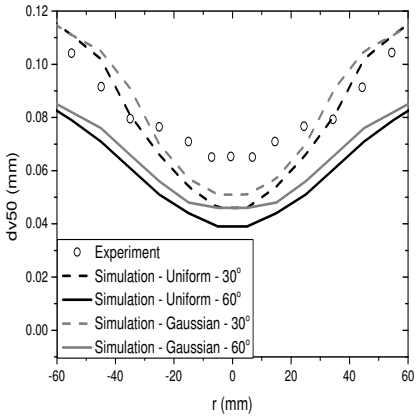

(c)

Fig. 8 Radial profiles of (a) volume flux, (b) axial velocity and (c) volume mean diameter of water droplets in the far field (y=260 mm)

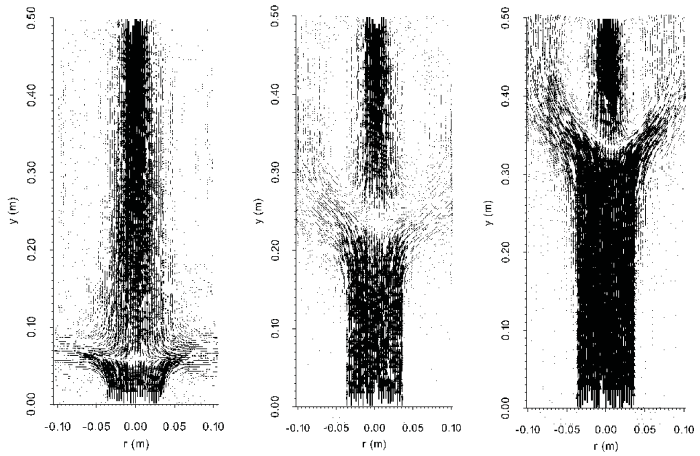

(a) (b) (c)

Fig. 9 Velocity vectors of the simulations for the interaction between the hot air plumes and the water spray for (a) 1.6, (b) 2.1 and (c) 2.6 kW with a 'Uniform' spray pattern and a 60^o degree injection angle.

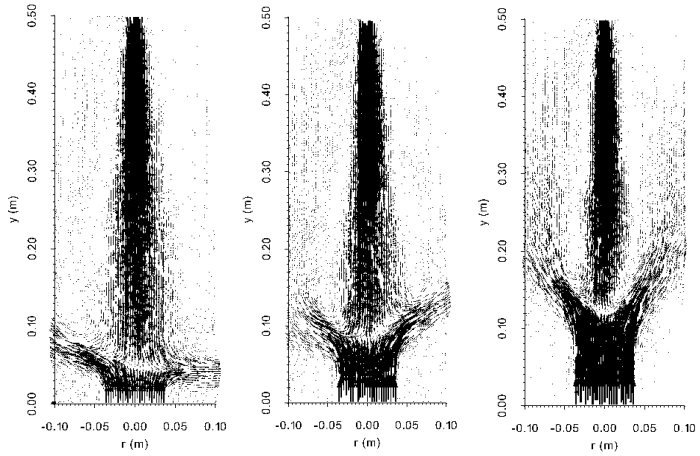

(a) (b) (c)

Fig. 10 Velocity vectors of the simulations for the interaction between the hot air plumes and the water spray for (a) 1.6, (b) 2.1 and (c) 2.6 kW with a 'Uniform' spray pattern and a 30^o degree injection angle.

where ρ_a is the density of the hot air plume, A_{nozzle} is the area of the nozzle (the hot air source) and v_a is the velocity of the air near the nozzle exit.

The area of the nozzle is calculated as:

$$A_{nozzle} = \frac{\pi D^2}{4} = \frac{\pi(0.074m)^2}{4} = 0.004m^2 \tag{25}$$

where D is the diameter of the hot air nozzle.

By inserting the velocity of the air near the exit nozzle for the three thermal powers, (i.e. 3.3, 4.2 and 5.3 m/s) and assuming the density of the air at 205^{o}C to be 0.74 kg/m^3, the momentum of the hot air plumes for the 1.6, 2.1 and 2.6 kW will be 0.032, 0.052 and 0.083 N, respectively.

The initial momentum of the water sprays, M_w, is approximated using two different methods:

– method 1:

$$M_w = \rho_w A_o v_w^2 \tag{26}$$

where ρ_w is the density of water, A_o is the orifice diameter and v_w is the injection velocity of the spray.
The area of the orifice is:

$$A_o = \frac{\pi d_o^2}{4} = \frac{\pi(0.00033m)^2}{4} = 8.5 \times 10^{-8} m^2 \tag{27}$$

where d_o is the orifice diameter.
The calculated injection velocity of sprays, v_w, is around 26.4 m/s and ρ_w = 1000 kg/m^3. Therefore, the initial momentum of the sprays is calculated to be 0.059 N.

– method 2:

$$M_w = \frac{\sqrt{2\rho_w \dot{V}_w^2}}{K} \tag{28}$$

where $\dot{V}_w$ is the volumetric flow rate of water and K is the k factor of the nozzle. The K factor is expressed as:

$$K = \frac{\dot{V}_w}{\sqrt{\Delta P}} \tag{29}$$

Combining Eqs. (28) and (29), M_w is calculated as:

$$M_w = \dot{V}_w \sqrt{2\rho_w \Delta P} \tag{30}$$

By considering the operating pressure, $p = 750$ kPa and the volume flow rate, $\dot{V}_w = 1.4 \times 10^{-6}$ m^3/s (0.084 lpm), the initial momentum of the sprays is calculated to be 0.054 N. Both values are notably higher than the one stated in the experiment, (0.043 N), approximated from the nozzle discharge rate and the injection velocity. Unfortunately, it is not totally clear how the initial water spray momentum was calculated in the experiments.

8 Conclusions

Large eddy simulations of water spray-hot air jet plume interactions with FireFOAM 2.2.x have been presented. Three hot air jet plumes with convective heat release rates of 1.6, 2.1 and 2.6 kW have been examined, interacting with a water spray with discharge rate of 0.084 lpm. A comparison between simulations and experiments involving only the hot air jet plumes, the water spray alone and the their interaction has been performed in order to evaluate the predictive capabilities of FireFOAM for such scenarios.

As a first observation, the results demonstrated that FireFOAM is capable of predicting well the mean values of the hot air jet plumes. The velocity fluctuations were under-estimated in the near-field region and over-predicted at higher locations. This might be due to the inlet boundary conditions (uniform velocity and random fluctuations have been used here). In the ceiling jet region, the maximum velocities and the boundary layer thicknesses were in good agreement with the experiments.

A second finding is that the predictions of FireFOAM with the reported injection angle for the water spray deviate from the experiments. Increasing the injection spray angle to match the experimental measurements close to the nozzle significantly affects the spray characteristics and overall improves the predictions. The spray pattern used in the numerical simulations also had a substantial influence on the spray predictions with the use of a uniform-like pattern giving predictions that were closer to the experimental data as opposed to the use predictions obtained with the use of a Gaussian-like pattern. Nevertheless, further research related to the injection method of droplets and the droplet distribution within the spray angle would be needed in order to draw firm conclusions on the discrepancies observed between the numerical simulations and the experiments.

The interaction between the hot air jet plumes and the water spray was characterized by the location of the interaction region. The influence of the injection angle in this case was substantial. The numerical predictions were only comparable to the experiments only when the injection angle was significantly increased (i.e. by back-calculating it based on the experimental data). It was shown that the interaction boundary moves up from the base of the plume with increasing convective heat release rates. The simulations followed the experimental trend but deviated up to 26% due to differences in both the predicted hot air jet plume and spray characteristics.

Several sub-models related to the spray simulations, such as vaporization, dispersion and injection models and droplet distribution at the injection point, need to be further investigated. Unfortunately, not many experimental data are available on spray-plume interaction, and there is lack of detailed information on characteristics of a fire plume and water spray during the interaction. It is therefore, crucial to carry out more experiments in order to extend the (few) existing studies in this area and consequently provide more data for the numerical modeling. Further evaluation of the predictive capabilities of FireFOAM for water spray-hot air jet plume interactions, by considering more experiments with well-known boundary conditions and experimental uncertainties, would be desirable in order to validate the code in a wide range of scenarios.

Acknowledgements

This research has been conducted within the PREdiction of Turbulent REactive Flows (PRETREF) project (http://www.pretref.ugent.be) and has been funded by Ghent University (Belgium) through GOA project BOF16/GOA/004. Dr. Tarek Beji is a post-doctoral fellow of the Fund of Scientific Research - Flanders (Belgium) (FWO Vlaanderen). Technical support from FM Global regarding the water spray modelling in FireFOAM is greatly acknowledged.

Compliance with Ethical Standards

Conflict of Interest: The authors declare that they have no conflict of interest.

References

1. B. Merci, T. Beji, Fluid mechanics aspects of fire and smoke dynamics in enclosure, Taylor and Francis Group, London, UK, 2016.
2. G. Grant, J. Brenton, D. Drysdale, Fire suppression by water sprays, Prog. Energy Combust. Sci., 26, 79-130, 2000.
3. L. Iannantuoni, D. Ettorre, G. Manzini, L. Araneo, Validation and assessment of a water mist multi-hole nozzle model for fire simulations, Fire Technol., 50, 505-524 (2013)
4. T. Sikanen, J. Vaari, S. Hostikka, A. Paajanen, Modeling and simulation of high pressure water mist systems, Fire Technol., 50, 483-504 (2014)
5. T. Beji, S. Ebrahimzadeh, G. Maragkos, B. Merci, Influence of the particle injection rate, droplet size distribution and volume flux angular distribution on the results and computational time of water spray CFD simulations, Fire Saf. J., 91, 586-595 (2017)
6. S.C. Kim, H.S. Ryou, An experimental and numerical study on fire suppression using a water mist in an enclosure, Building Environ., 38, 1309-1316 (2003)
7. R.A. Hart, Numerical modelling of tunnel fires and water mist suppression, PhD thesis, University of Nottingham, 2005.
8. K.V. Meredith, P. Chatterjee, Y. Wang, Y. Xin, Simulating sprinkler based rack storage fire suppression under uniform water application, 7th International Seminar on Fire and Explosion Hazards, Providence, RI, 2013.
9. K.V. Meredith, X. Zhou, S. Ebrahimzadeh, B. Merci, Numerical simulation of spray-plume interactions, 9th U. S. National Combustion Meeting , Cincinnati, Ohio, 2015.
10. D.T. Sheppard, Spray characteristics of fire sprinklers, US Department of Commerce, National Institute of Standards and Technology, 2002.
11. W.K. George, R.L. Alpert, F. Tamanini. Turbulence measurements in an axisymmetric buoyant plume, Int. J. Heat Mass Transf., 20, 1145-1154 (1977)
12. A. Shabbir, W.K. George, Experiments on a round turbulent buoyant plume, J. Fluid Mech., 275, 1-32 (1994)
13. J. Hua, K. Kumar, B. C. Khoo, H. Xue, A numerical study of the interaction of water spray with a fire plume. Fire Saf. J., 37, 631-657 (2002)
14. X. Zhou, K.H. Luo, J.J.R. Williams, Large-eddy simulation of a turbulent forced plume, European Journal of Mechanics - B/Fluids, 20, 233-254 (2001)
15. J. Worthy, P. Rubini, A study of les stress and flux models applied to a buoyant jet, Numerical Heat Transfer, Part B: Fundamentals, 48, 235-256 (2005)
16. Z.H. Yan. Large eddy simulations of a turbulent thermal plume, Heat and Mass Transfer, 43, 503-514 (2007)
17. G. Maragkos, P. Rauwoens, Y. Wang, B. Merci, Large eddy simulations of the flow in the near-field region of a turbulent buoyant helium plume, Flow Turbul. Combust., 90, 511-543 (2013)
18. Y. Xin, J. Gore, K.B. McGrattan, R.G. Rehm, H.R. Baum, Large eddy simulation of buoyant turbulent pool fires, Proceedings of the Combustion Institute, 29, 259-266 (2002)
19. J. Worthy, P. Rubini, Large eddy simulation of buoyant plumes, 4th International Seminar on Fire and Explosion Hazards, Londonderry, UK, 2003.
20. X. Zhou, Characterization of interactions between hot air plumes and water sprays for sprinkler protection, Proc. Comb. Inst., 35, 2723-2729 (2015)
21. X. Zhou, PIV measurements of velocity fields of three hot air jet plumes impinging on a horizontal ceiling, 10^{th} Asia-Oceania Symposium on Fire Science and Technology, Tsukuba, Japan, 2015.
22. R.L. Alpert, Turbulent ceiling-jet induced by large-scale fires, Combust. Sci. Technol., 11, 197-213 (1975)
23. H.Z. You, G.M. Faeth, An investigation of fire impingement on a horizontal ceiling, Pennsylvania State University, Department of Mechanical Engineering, 1981.
24. H-C. Kung, H-Z. You, R.D. Spaulding, Ceiling flows of growing rack storage fires, Proceedings of the Combustion Institute, 21, 121-128 (1986)

25. P. Chatterjee, K.V. Meredith, B. Ditch, H-Z. Yu, Y. Wang, F. Tamanini, Numerical simulations of strong-plume driven ceiling flows, Fire Safety Science, 11, 458-471 (2014)
26. L.Y. Cooper, The interaction of an isolated sprinkler spray and a two-layer compartment fire environment, Int. J. Heat Mass Transf., 38, 679-690 (1995)
27. J.A. Schwille, R.M. Lueptow, The reaction of a fire plume to a droplet spray, Fire Saf. J., 41, 390-398 (2006)
28. H-C. Kung, B. Song, Y. Li, X. Liu, L. Tian, B. Yang, Sprinkler protection of non-storage occupancies with high ceiling clearance, Fire Saf. J., 54, 49-56 (2012)
29. R.G. Bill, Numerical simulation of actual delivered density (ADD) measurements. Fire Saf. J., 20, 227-240 (1993)
30. R.L. Alpert, Numerical modeling of the interaction between automatic sprinkler sprays and fire plumes, Fire Saf. J., 9, 157-163 (1985)
31. S. Nam, Numerical simulation of the penetration capability of sprinkler sprays, Fire Saf. J., 39, 307-329 (1999)
32. S. Nam, Development of a computational model simulating the interaction between a fire plume and a sprinkler spray, Fire Saf. J., 26, 1-33 (1999)
33. A.H. Lefebvre, Atomization and sprays, Hemisphere Pub., 1989.
34. N. O'Grady, V. Novozhilov, Large eddy simulation of sprinkler interaction with a fire ceiling jet, Combust. Sci. Technol., 181, 984-1006 (2009)
35. T. Poinsot, D. Veynante, Theoretical and Numerical Combustion, Edwards, 2012.
36. P. Moin, K. Squires, W. Cabot, S. Lee, A dynamic subgrid-scale model for compressible turbulence and scalar transport, Phys. Fluids A, 3, 2746-2757 (1991)
37. G. Maragkos, T. Beji, B. Merci, Advances in modelling in CFD simulations of turbulent gaseous pool fires, Combust. Flame, 181, 22-38 (2017)
38. K.K. Kuo, Recent Advances in Spray Combustion, Volumes I and II, AIAA, 1996.
39. W.E. Ranz, W.R. Marshall, Evaporation from Drops, Chem. Eng. Prog., 48, 141-146 (1952)
40. R. Bird, W. Stewart, W. Lightfoot, Transport phenomena, Wiley, 1960.
41. G.B. Macpherson, N. Nordin, H.G. Weller, Particle tracking in unstructured, arbitrary polyhedral meshes for use in cfd and molecular dynamics, Comm. Numer. Methods Engrg. 25, 263-273 (2008)
42. N. Nordin, Complex chemistry modelling of diesel spray combustion, PhD thesis, Chalmers University of Technology, Sweden, 2001.
43. F.P. Kärrholm, Numerical Modelling of diesel spray injection, turbulence interaction and combustion, PhD thesis, Chalmers University of Technology, Sweden, 2008.
44. S. Ebrahimzadeh, Extensive Study of the Interaction of a Hot Air Plume with a Water Spray by Means of CFD Simulations, PhD thesis, Ghent University, Belgium, 2016.
45. M.L. Bullen, The effect of a sprinkler on the stability of a smoke layer beneath a ceiling, Fire Research Note 1016, pages 1-11, 1974, Borehamwood, UK, Fire Research Section.
46. Z. Tang, J. Vierendeels, Z. Fang, B. Merci, Description and application of an analytical model to quantify downward smoke displacement caused by a water spray, Fire Saf. J., 55, 50-60 (2013)
47. Z. Tang, Z. Fang, B. Merci, Development of an analytical model to quantify downward smoke displacement caused by a water spray for zone model simulations, Fire Saf. J., 63, 89-100 (2014)